Fe2.5Co0.3Zn0.2O4/CuCr-LDH as a visible-light-responsive photocatalyst for the degradation of caffeine, bisphenol A, and simazine in pure water and real wastewater under photo-Fenton-like degradation process

Arezou Fazli, Marcello Brigante, Alireza Khataee, Gilles Mailhot

$Fe_{2.5}Co_{0.3}Zn_{0.2}O_4$/CuCr-LDH as a visible-light-responsive photocatalyst for the degradation of Caffeine, Bisphenol A, and Simazine in pure water and real wastewater under photo-Fenton-like degradation process

Arezou Fazli[a, b], Marcello Brigante[a], Alireza Khataee[b,c*], Gilles Mailhot[a*]

[a] *Université Clermont Auvergne, CNRS, SIGMA Clermont, Institut de Chimie de Clermont-Ferrand, F-63000 Clermont-Ferrand, France*

[b] *Research Laboratory of Advanced Water and Wastewater Treatment Processes, Department of Applied Chemistry, Faculty of Chemistry, University of Tabriz, 51666-16471, Tabriz, Iran*

[c] *Department of Environmental Engineering, Gebze Technical University, 41400 Gebze, Turkey*

* Corresponding authors:

a_khataee@tabrizu.ac.ir (A. Khataee)
gilles.mailhot@uca.fr (G. Mailhot)

Abstract

This paper outlines the synthesis and application of a sustainable composite for the photo-Fenton-like degradation of caffeine, bisphenol A, and simazine. The phase, morphology, optical and magnetic properties of the samples were evaluated by different characterization techniques. The composite of $Fe_{2.5}Co_{0.3}Zn_{0.2}O_4$ and copper-chromium layered double hydroxide (CuCr-LDH) was determined to be the most favorable photocatalyst in the photo-Fenton-like process when compared with Fe_3O_4, $Fe_{2.5}Co_{0.3}Zn_{0.2}O_4$, CuCr-LDH, and Fe_3O_4/CuCr-LDH composite. Studying the efficiency of the photo-Fenton-like degradation process in the presence of the $Fe_{2.5}Co_{0.3}Zn_{0.2}O_4$/CuCr-LDH composite revealed a degradation rate constant of caffeine twice more than the sum of those obtained for the individual processes. This ascribes to the synergistic effect by which the photo-generated electron-hole from the catalyst and the efficient reduction of Fe^{3+}, Cu^{2+}, etc. during the photo-Fenton-like reaction is accelerated. Moreover, under the optimal condition and after 120 min of heterogenous photo-Fenton-like process at natural pH, > 90% of pollutants mixture was decomposed. The experiments fulfilled in near-real conditions demonstrated I) the high stability and magnetically recoverability of the photocatalyst and II) the proper degradation performance of the applied heterogenous photo-Fenton-process in the removal of pollutant mixture in different water bodies and in the presence of chloride and bicarbonate ions.

Keywords: Sustainable photocatalyst; CuCr-LDH; Doped magnetite; Mineralization; Micropollutants mixture.

1. Introduction

Industrial toxic wastes like pharmaceuticals, pesticides, and phenols are present in water and wastewater, which turned into a globally concerning issue. Caffeine (CAF) is a widely used psychoactive medicine and it can be found in coffee seeds (0.43 to 0.82 mg/mL), tea leaves, etc. (Chen et al., 2018). Some industrial raw materials such as bisphenol A (BPA) are being used for the preparation of water bottles, food containers, and polycarbonates. Nevertheless, according to the World Health Organization (WHO), a low concentration of BPA can result in hypertension and cell disorders (Chen et al., 2020). Furthermore, different s-triazine herbicides have been used in the agriculture to manage the broadleaf and grassy weeds (X. Yang et al., 2020). Due to the excessive usage of the herbicides such as simazine (SIM), a different amount of them has appeared in groundwater which leads to DNA replication and disorders in the central nervous system (Nahim-Granados et al., 2020). Due to the entrance of the above-mentioned compounds to the water bodies, researchers have recently focused on the performance of various treatment processes for the degradation of an individual kind of pollutant (Hieu et al., 2021). However, it is well-known that real wastewater comprises a mixture of diverse kinds of pollutants which should be treated before their arrival into aquatic ecosystems (Chavan and Fulekar, 2020).

As the representative AOPs, the Fenton processes can activate H_2O_2 (HP) by the Fenton reagent Fe^{2+} to produce reactive $^{\bullet}OH$ (Brillas, 2020). So far, different inherent shortcomings such as higher efficiencies at acidic pHs and the rapid decay of the utilized catalyst confined their usage for practical applications (Zhang et al., 2020). To overcome these restrictions, the photo-Fenton processes in the presence of a photocatalyst is of great consideration. The photo-generated electron and hole pairs in the photocatalysts promote the regeneration of Fenton reagent Fe^{2+} which is favourable for the Fenton reactions (Sharma et al., 2020). In this context, a big effort has been devoted to design the effective heterogeneous photocatalysts grounded on

the advantages such as high activity in different pH values and efficient recovery from the reaction media (Sharma et al., 2020). Layered double hydroxides (LDHs) are a class of two-dimensional (2D) synthetic compounds with a high specific structure and chemical stability which make them suitable candidates for the varied catalytic degradation processes (Wu et al., 2022). For instance, Bai et al. (Bai et al., 2017) and Li et al. (Li et al., 2020) used Co-Fe-LDH and Zn-Al-LDH as Fenton and photo-Fenton catalysts to degraded different water pollutants, respectively. Besides the higher photocatalytic activity, recoverability and reusability of the nanoscale photocatalysts after degradation reactions are of great consideration for sustainable process management (Fazli et al., 2021b). In order to recover LDHs from the reaction media by a permanent magnet, different LDH heterojunctions with magnetic materials have been synthesized and used in AOPs (Gonçalves et al., 2019).

In previous work, the activation of persulfate and HP in the presence of $Fe_{2.5}Co_{0.3}Zn_{0.2}O_4$ nanoparticles to decompose a pharmaceutical water pollutant was studied. It was found out that the nanoparticles were magnetically separable; however, under UVA illumination and the solution pH of 8, the co-doped magnetite had lower efficiency for the activation of HP (Fazli et al., 2021b). Therefore, it would be of great importance to add a highly active semiconductor to co-doped magnetite to prepare a high-performance and environmentally friendly photocatalyst for the photo-Fenton-like process. Considering the reaction rate constant of Fe (III) (10^{-3}–10^{-2} M^{-1} s^{-1}), Fe (II) (76 M^{-1} s^{-1}), Cu (I) (10^4 M^{-1} s^{-1}) and Cu (II) (4.6×10^2 M^{-1} s^{-1}), copper can react with HP faster (Xiao et al., 2020). Moreover, previous works have confirmed the high impact of chromium on the further production of hydroxyl radicals in the UV/Fenton system (Liang et al., 2012). Therefore, herein, we synthesized a CuCr-LDH as the proper semiconductor and merged its merits with the magnetically separable $Fe_{2.5}Co_{0.3}Zn_{0.2}O_4$ nanoparticles to prepare an efficient visible-light-responsive photocatalyst for the photo-Fenton-like degradation of 3 kinds of water contaminants. To the authors' knowledge, no

research was devoted to studying the effect of $Fe_{2.5}Co_{0.3}Zn_{0.2}O_4$/CuCr-LDH composite in the photo-Fenton-like degradation of pollutant mixture in pure water and real wastewater. Therefore, the proposed research study was undertaken with the following goals: a) to prepare a visible-light responsive magnetic composite ($Fe_{2.5}Co_{0.3}Zn_{0.2}O_4$/CuCr-LDH); (b) investigate the optical, magnetic, and physicochemical properties of the composite, (c) study the performance of the so-synthesized photocatalysts for the photo-Fenton-like degradation of water pollutants, (d) examine the stability and reusability of so-synthesized photocatalyst, (e) investigate the effect of inorganic anions and radical scavengers, (f) assess the performance of composite as the photo-Fenton-like photocatalyst for the effective degradation of pollutants mixture in pure and tap water, as well as real wastewater matrix, and finally (g) examine the efficiency of the photo-Fenton-like process for the mineralization of the pollutants mixture.

2. Experimental

2.1. Materials

$CoCl_2 \cdot 6H_2O$ 97%, $NaNO_3$ 99%, $FeCl_2 \cdot 4H_2O$ 99%, $ZnCl_2 \cdot 4H_2O$ 98%, HCl 38%, $N_2H_4 \cdot H_2O$ 90–100%, NaOH 99%, $Cu(NO_3)_2 \cdot 3H_2O$ 99%, $Cr(NO_3)_3 \cdot 9H_2O$ 99%, H_2O_2 30%, KI 99.5%, $NaHCO_3$, 99.7%, NaCl, 99% and organic solvents (purity greater than 99%) were provided from Sigma Aldrich France and used with no further purification.

2.2. Preparation of the photocatalysts

The required solutions were prepared with previously deoxygenated distilled water via argon gas. The typical procedure to synthesize the $Fe_{2.5}Co_{0.3}Zn_{0.2}O_4$/CuCr-LDH composite is summarized in Fig. S1. As the first step, we synthesized Co and Zn co-doped Fe_3O_4 nanoparticles by applying the method explained in our previous work (Fazli et al., 2021c). In this regard, a 100 mL solution comprised of $FeCl_2$. H_2O, $ZnCl_2$. $4H_2O$, and $CoCl_2$. $6H_2O$ and

10 mL of HCl (0.6 M) was prepared and added to the three-neck flask. The solution was stirred at 500 rpm, and then 1 mL hydrazine was added to the solution to reach lower solution pH. Afterward, the alkaline solution comprised of $NaNO_3$ (0.9 M) and NaOH (0.4 M), was added drop by drop to the solution. After the addition of the alkaline solution with the speed of 3 drops/second, the mixture was stirred for 2 h at 95 ºC. The resulted particles were magnetically collected, washed three times with distilled water, and finally dried at 90 °C for 24 h.

In the following, the obtained nanoparticles were used to prepare the $Fe_{2.5}Co_{0.3}Zn_{0.2}O_4$/CuCr-LDH composite. For this purpose, two separated solutions (I and II) were prepared as follows: Solution I: 0.5 g of the so-synthesized co-doped magnetite was dispersed in 150 mL of water for 30 min; after that, 150 mL of NaOH (2 M) was added drop by drop. At the same time, the specific amount of Cr $(NO_3)_3.9H_2O$ (0.25 M) and Cu $(NO_3)_2.3H_2O$ (0.5 M) were respectively dissolved in 50 and 100 mL of distilled water and mixed with each other to prepatre a solution of 150 mL as the salts solution (II). Thereafter, solutions I and II were mixed drop by drop; while, the mixture was vigorously stirring and the pH was being kept between 9.3 and10. The final mixture was aged for 24 h. As the final step, the particles of the composite were magnetically separated, rinsed three times with water, and dried at 60 °C for 12 h. Pure CuCr-LDH was prepared with the same procedure without adding co-doped Fe_3O_4.

2.3. Characterization

X-ray diffraction (XRD, D8 Advance, Bruker, Germany) and X-ray photoelectron spectroscopy (XPS, OMICRON EA125, Germany) were utilized to investigate the structural properties of the samples. SEM (Tescan Mira3, Czech Republic, equipped with a Zeiss Sigma 300) and TEM (H-7650, AMT40, Germany) were used to studying the surface morphology of the samples. Also, a 3 Flex instrument (Micromeritics, USA) was used to determine the surface area of the prepared nanomaterials based on the adsorption-desorption isotherms. UV–visible

151 diffuse reflectance spectrophotometry (UV-Vis DRS, S 250, Germany) and a vibrating sample
152 magnetometer (VSM, Lakeshore, 7400 Series) were used to study the optical and magnetic
153 aspects of the prepared nanoparticles.
154

155 ## 2.4. Photo-Fenton-like catalytic tests

156 According to the picture inserted in Fig. S1, all the experiments were carried out in a 50 mL
157 Pyrex cylindrical photocatalytic reactor. Meanwhile, a solar simulator lamp (Ocean optics)
158 fitted with cut-off filters at $\lambda \geq 400$ nm was used to simulate the vis-light. Fig. S2 shows the
159 emission spectra related to the abovementioned lamp with and without using a filter. The light
160 source was placed at a 15 cm distance from the reactor. In order to control the temperature, a
161 water circulator system was embedded around the reactor. For each run, 50 mL of pollutants
162 solution with the concentration of 50 μM was prepared and after adding a certain amount of
163 catalyst the pH of the solution was adjusted to be 8. Prior to irradiation, the minimum time
164 needed for the maximum adsorption of organic pollutants on the surface of the catalyst was
165 studied by stirring the suspension in dark. It was found out that the maximum adsorption of
166 three target pollutants was reached approximately after 30 min of stirring. Therefore, after 30
167 min of stirring in dark, the predetermined amount of HP was added to the suspension and the
168 irradiation of the suspension was started. Several samples were collected after 15 min, filtered,
169 and passed to a vial with 20 μL of methanol to stop the possible reactions. A high-performance
170 liquid chromatography (Alliance, waters, USA) using a C18 column was applied for measuring
171 the concentration of remaining pollutants in the reaction media. UPLC condition: injection
172 volume of 10 μL, flow rate of 0.2 mL min^{-1}, and isocratic elution comprising of 40 %
173 acetonitrile and 60 % ultrapure water were used as the best method for the detection of
174 pollutants. The retention time for CAF, BPA, and SIM was found to be 1.4, 4.4, and 3 min,
175 respectively. The relative pollutant concentration (%) in the reaction was determined from the

decay of polutants as $\frac{C_t}{C_0}$ during the reaction time where C_0 and C_t are the intial concentration and remaining concetration at time t, respectively. The reusability of the composite was studied by collecting it after each degradation run and reusing it for other runs. Moreover, a TOC analyzer (Shimadzu, TOC-L, Japan) was used for monitoring the mineralization of pollutants. The dissolved concentrations of Cu, Cr, Fe, Co, and Zn were measured by an inductively coupled plasma emission spectroscopy (ICP-AES, Jobin-Yvon ULTIMA C, USA). The real wastewater was obtained at the outlet of the treatment from the "3 rivières" urban STP, Clermont-Ferrand, France in December 2019 and main physico-chemical parameters are reported elsewhere (Fazli et al., 2021c).

3. Results and discussion

3.1. Characterization

3.1.1. Phase analysis: XRD and XPS

The XRD patterns of the so-synthesized samples were plotted together for comparison in Fig. 1. From the results, it is evident that the obtained positions of peaks for co-doped magnetite are consistent with the standard diffraction data for magnetite (JCPDS file no. 01–089-0951) (Fazli et al., 2021c). Furthermore, the XRD pattern related to the $Fe_{2.5}Co_{0.3}Zn_{0.2}O_4$/CuCr-LDH composite proved the existence of the specific peaks at the 2θ values of 18°, 30.05°, 35.9°, 36.7°, 43.6°, 54.1°, 57.5°, and 62.5° relating to the co-doped magnetite and also the peaks at 10.66°, 21°, 35.1°, 38°, 47.05°, 60.05°, and 61.5° corresponding to CuCr-LDH (JCPDS file no. 00-035-0965) (Aghaziarati et al., 2020). The co-existence of the related peaks proved that the phase of co-doped magnetite and LDH are well coupled with each other. In addition, no more irrelevant peaks were observed in the XRD pattern of the composite, which revealed the purity and crystallinity of the sample. However, in comparison with pure $Fe_{2.5}Co_{0.3}Zn_{0.2}O_4$

200 nanoparticles and LDH, the intensity of the related peaks in the XRD pattern of the composite
201 was mitigated. This phenomenon has been widely related to the weak crystallinity nature of the
202 composite arising from the formation of heterojunction between $Fe_{2.5}Co_{0.3}Zn_{0.2}O_4$ and co-doped
203 magnetite.
204 Furthermore, the high-resolution XPS (HRXPS) spectra of the so-synthesized
205 nanocomposite have been presented in Fig. 1. Considering the observed sub-peaks, the binding
206 energies of 710.57 and 724.02 eV ascertain the existence of Fe (II), while the related peaks for
207 Fe (III) are located in the 712.40 and 726.10 eV (Fazli et al., 2021c). The observed satellite
208 (shoulder) peaks are in coherence with the reported results of the other researchers (Rad et al.,
209 2018; Yamashita and Hayes, 2008) and affirm the presence of Fe (II). Moreover, the spectrum
210 corresponding to Co $2p_{1/2,}$ Co $2p_{3/2}$ revealed the presence of Co (II) (781.53 eV and 796.71 eV)
211 and Co (III) (780.6 eV) on the surface of the composite (Chen et al., 2014). The existence of
212 Zn $2p_{3/2}$ and Zn $2p_{1/2}$ were affirmed with the binding energies at 1019.99 eV and 1040.57 eV
213 (Nguyen et al., 2021), respectively. Furthermore, considering the HRXPS peak related to Cu
214 2p, the signals of Cu (II) was observed at 954.63 eV (Liu et al., 2016; Wu et al., 2006). An other
215 peak at 934.68 eV also confirmed the presence of Cu (II) (Liu et al., 2016; Wu et al., 2006). It
216 is worth noting that the satellite peaks characterize the materials which possess a d^9
217 configuration in the ground state (Wu et al., 2006). Concerning this fact, the appeared peaks at
218 941.79 eV, 944.14 eV, and 962.20 eV relate to the $3d^9$ shell of Cu (II) (Liu et al., 2016). Finally,
219 Cr (III) has been recognized by the peaks positioned at the emerged peaks at 575.96 eV and
220 585.57 eV for Cr 2p.
221

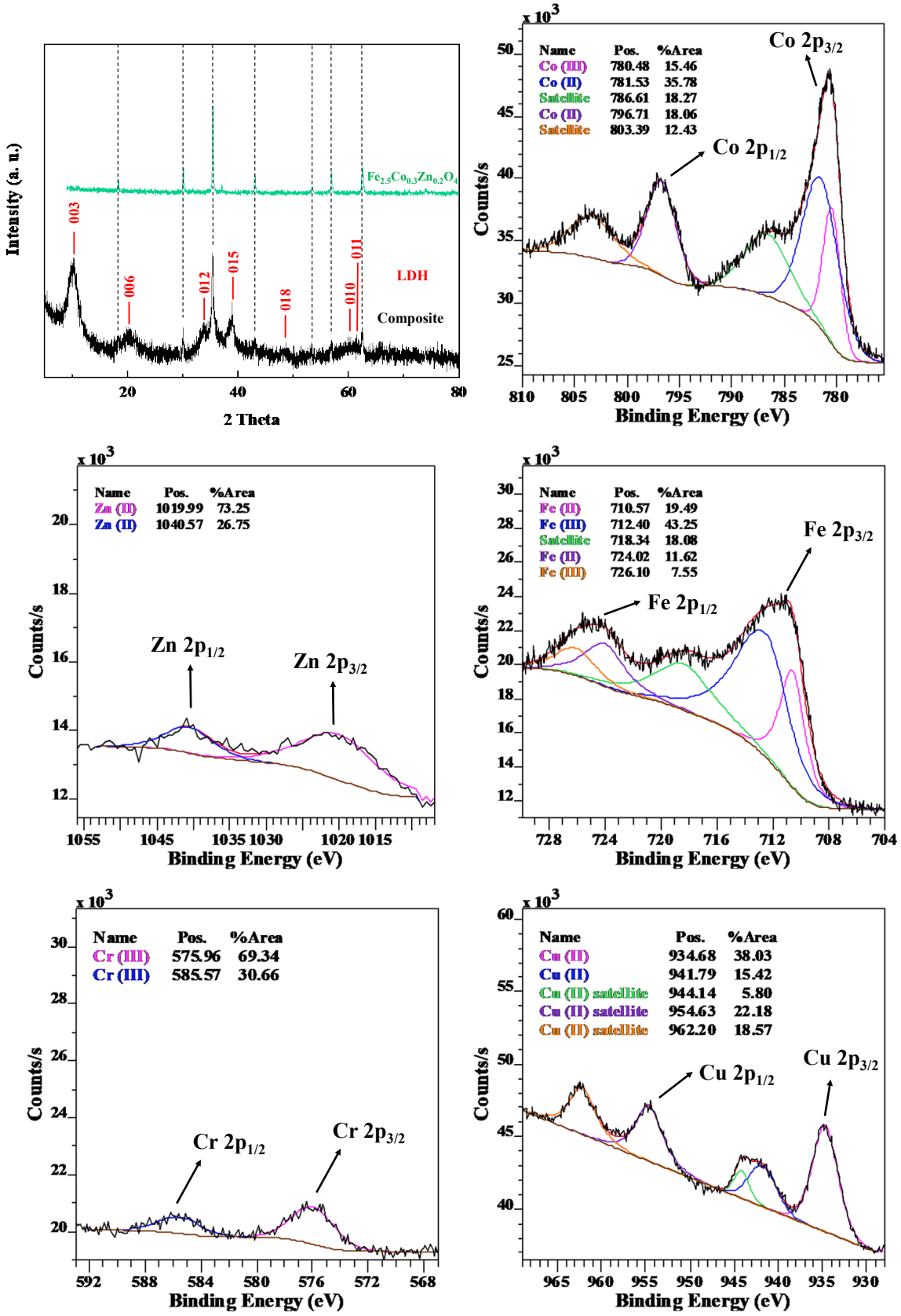

Fig. 1. XRD 2θ scans for the so-synthesized photocatalysts and high-resolution XPS spectra of Fe 2p, Zn 2p, Co 2p, Cu 2p, and Cr 2P of $Fe_{2.5}Co_{0.3}Zn_{0.2}O_4$/CuCr-LDH composite.

3.1.2. Morphological analysis

Fig. S3 (a-c) shows the SEM images of $Fe_{2.5}Co_{0.3}Zn_{0.2}O_4$, CuCr-LDH, and $Fe_{2.5}Co_{0.3}Zn_{0.2}O_4$/CuCr-LDH composite. The cubic and lamellar structures were observed for the co-doped magnetite and pure LDH, whereas, the SEM image corresponding to the composite revealed the coverage of co-doped magnetite nanoparticles with the LDH layers. This was further proved by the TEM images (Fig. S3 (d-e)) and SEM elemental mapping. According to the magnified TEM image of the composite, the composite consists of the cubic co-doped magnetite and layers of Cu-Cr-LDH. Notably, Fig. 2 depicts the EDX spectra with the relative weight and atomic percentage of the elements.

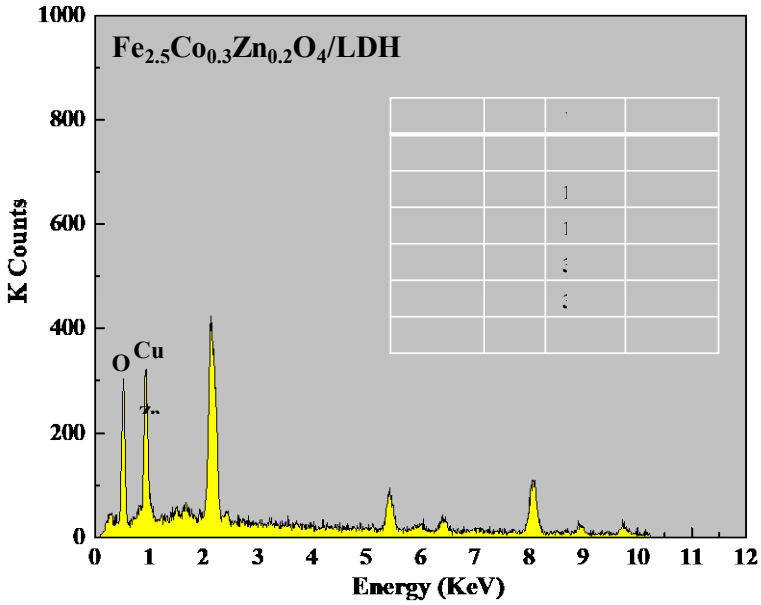

Fig. 2. The EDX spectrum of the $Fe_{2.5}Co_{0.3}Zn_{0.2}O_4$/CuCr-LDH composite.

Moreover, based on Fig. 3 which present the SEM elemental mapping it can be deduced that the composite contains the elements such as Co, Cr, Cu, Zn, and Fe which have been uniformly distributed on the surface.

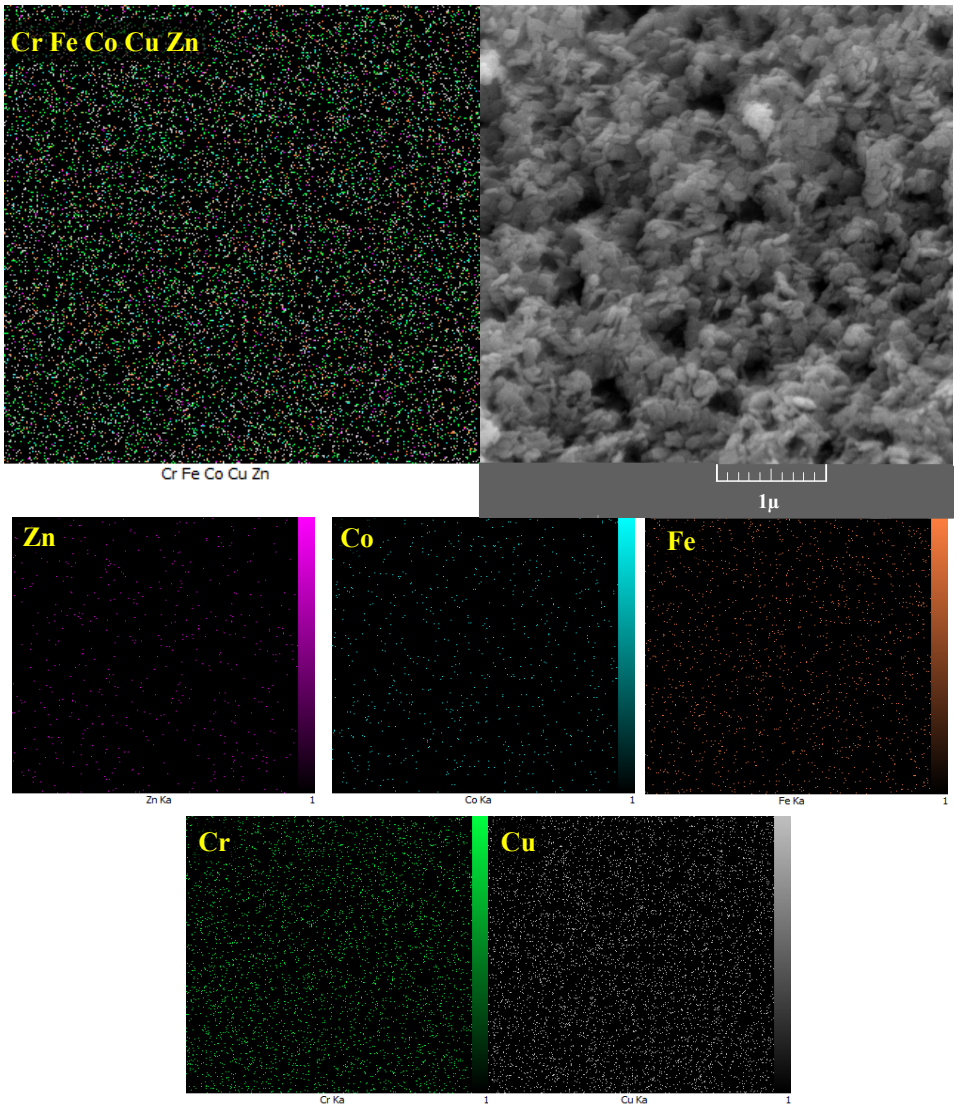

Fig. 3. SEM elemental mapping of the $Fe_{2.5}Co_{0.3}Zn_{0.2}O_4$/CuCr-LDH.

Furthermore, the surface area, the volume of gas adsorbed (Vm) at standard temperature and pressure, and pore volume extracted from the BET plot are inserted in Table 1. Accordingly, the specific surface area of the composite was the largest, which in turn results in the higher contribution of its surface in the photocatalytic degradation reactions. On the other hand, V_m was increased in the order of co-doped < LDH < composite, depicting the higher porosity of the sample. Moreover, it should be noted that the obtained pore volume of the $Fe_{2.5}Co_{0.2}Zn_{0.3}O_4$/CuCr-LDH composite is relatively higher than those reported for other composites such as NiFe-LDH/rGO (Khataee et al., 2019) and magnetic Mg-Fe/LDH

intercalated activated carbon (Alagha et al., 2020), which acknowledges the mesoporous characterization of the so-synthesized composite (Alagha et al., 2020).

Table 1. Textural properties of the so-synthesized samples extracted from the BET plot.

Samples	S_{BET} (m^2 g^{-1})	V_m (cm^3 (STP) g^{-1})	V_P (cm^3 g^{-1})
$Fe_{2.5}Co_{0.3}Zn_{0.2}O_4$	19.98	4.6	0.32
Pure CuCr-LDH	43.21	9.64	0.28
$Fe_{2.5}Co_{0.3}Zn_{0.2}O_4$/CuCr-LDH	74.21	17.21	0.39

3.1.3. Optical and magnetic properties

To investigate the light response of the so-synthesized nanomaterials the UV–vis DRS analysis was applied. It was proved that the doped elements such as Co and Zn could modify the redox properties of the pure magnetite by preparing the oxygen vacancies in the magnetite structure which favors the electron capture (Fazli et al., 2021c). However, the prepared photocatalyst was not active under visible light irradiation. Considering Fig. S4, the composite of $Fe_{2.5}Co_{0.3}Zn_{0.2}O_4$ nanoparticles with the CuCr-LDH enhanced the visible light absorption capacity. In conclusion, the effective light-absorbing capability of the composite could be aroused from two main facts: (I) the promoted photocatalytic efficiency of magnetite by doping Zn and Co metal ions to its structure, and (II) the inherent visible light absorption ability of CuCr-LDH compared to the magnetite nanoparticles could narrow the bandgap and raise the optical response of the final composite (Nguyen et al., 2021). The bandgap energies were estimated using the Kubelka-Monk formula and Tauc's plot (Rad et al., 2018). The $(\alpha h\nu)^2$-$h\nu$ curves of the samples were displayed in Fig. S4. Using tangent line to the curves shown in Fig. S4, the bandgap of $Fe_{2.5}Co_{0.3}Zn_{0.2}O_4$ nanoparticles, CuCr-LDH, and $Fe_{2.5}Co_{0.3}Zn_{0.2}O_4$/CuCr-LDH composite was found to be 2.78, 2.69, and 1.66, respectively. The results confirmed the existence of a redshift in the absorbance spectrum of the composite which could be the main

role in its greater excitation under the visible light irradiation to generate reactive electron-hole. In our previous work (Fazli et al., 2021a), we realized that the combination of pure magnetite and layered double hydroxide results in the effective electron transfer on the surface of the composite leading to the lower recombination rate of the electron and holes. Consequently, the low bandgap as well as the efficient electron transfer on the surface of the $Fe_{2.5}Co_{0.3}Zn_{0.2}O_4$/CuCr-LDH composite results in the increased production and availability of the electrons on its surface.

In our previous work, we observed that Fe_3O_4 preserved its magnetic properties even after co-doping of Zn and Co in its structure (Fazli et al., 2021c). In addition, the magnetic properties of the prepared composite were evaluated by applying a systematic magnetization measuring as a function of the used field. Fig. 4 shows that the appraised value for the magnetization saturation (M_s) of $Fe_{2.5}Co_{0.3}Zn_{0.2}O_4$/CuCr-LDH composite was 56.14 emu g^{-1}, indicating that the so-synthesized nanomaterial is a ferromagnetic phase (Kiziltaş et al., 2020). Hence, this magnetic behavior allowed the composite to be separated from the reaction media by applying an external magnetic field (inserted photo in Fig. 4).

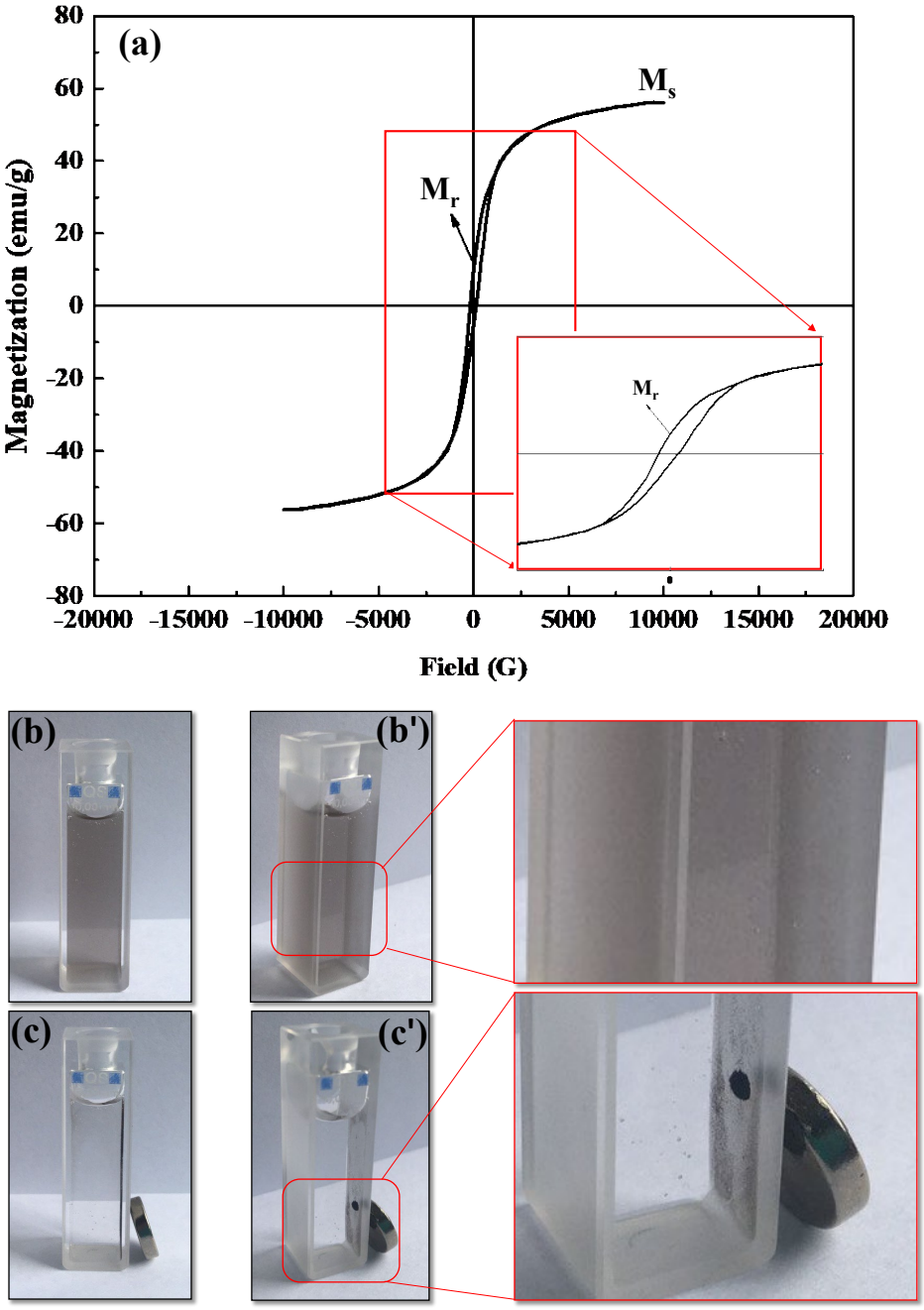

Fig.4. (a) The VSM plot of the so-synthesized $Fe_{2.5}Co_{0.3}Zn_{0.2}O_4$/CuCr-LDH composite, the front and side images of a spectrophotometer cell containg the suspention of $Fe_{2.5}Co_{0.3}Zn_{0.2}O_4$/CuCr-LDH composite before (b-b') and after (c-c') applying an external magnetic field.

3.2. Impact of different oxidation processes

CAF was used as a model pollutant for evaluating the photo-Fenton-like degradation performance using $Fe_{2.5}Co_{0.3}Zn_{0.2}O_4$, CuCr-LDH, and $Fe_{2.5}Co_{0.3}Zn_{0.2}O_4$/CuCr-LDH composite under visible-light irradiation. Moreover, for better evaluation of their photocatalytic activity, the previously synthesized and characterized pure magnetite (Fazli et al., 2021c) and its composite with CuCr-LDH (Fazli et al., 2021a) was also used (Fig. S5). Before starting the photo-Fenton-like reactions, the adsorption trend of 50 μM of CAF on the surface of the samples was studied. When the prepared solutions were stirred for 2 hours in the dark, the adsorption/desorption of CAF was equilibrated after 30 min (the results of 2 hours have not been reported). Therefore, in the case of stirring the solutions for 2h in the dark, the CAF adsorption percentage of 0.15, 2.46, 9.11, 0.05, and 2.7 % were achieved in the presence of Fe_3O_4, $Fe_{2.5}Co_{0.3}Zn_{0.2}O_4$, CuCr-LDH, Fe_3O_4/CuCr-LDH, and $Fe_{2.5}Co_{0.3}Zn_{0.2}O_4$/CuCr-LDH composite, respectively. According to the results presented in Fig. S5, pure and co-doped magnetite have almost no response under the visible light irradiation for the CAF degradation. Also, the pure layered double hydroxide has shown more adsorption of CAF rather than its degradation. Considering the results obtained from the BET analysis, the main reason for high adsorption in the presence of the layered double hydroxide can be related to its higher surface area. However, combined adsorption and photo-Fenton-like processes reduced C_t/C_0 of CAF, where the degradation efficiency was to be 41.6, and 66.4 % for Fe_3O_4/CuCr-LDH, and $Fe_{2.5}Co_{0.3}Zn_{0.2}O_4$/CuCr-LDH, respectively. The higher degradation efficiency of CAF in the presence of $Fe_{2.5}Co_{0.3}Zn_{0.2}O_4$/CuCr-LDH composite is in line with the obtained results from the DRS analysis. The Low bandgap of the composite (1.66 eV), as well as, the presence of structural defects and metal-semiconductor interface (Schottky interface) in co-doped magnetite/LDH resulted in the higher production and better transference of electrons. This phenomenon led to the production of more hydroxyl radicals in the presence of HP (Cao et al., 2021). Our results followed the similar sequence obtained by the other researchers. For instance,

Cao et al (Cao et al., 2021). reported that the $La_{0.7}Sr_{0.3}MnO_3$/α-Fe_2O_3 composite possesses the best photocatalytic behavior in comparison with the pure α-Fe_2O_3 and $La_{0.7}Sr_{0.3}MnO_3$. Xiao et al (Xiao et al., 2020) also reported that the composite of Cu doping magnetite with Cu/C showed higher degradation efficiency for Rhodamine-B in comparison with the sole components.

As the $Fe_{2.5}Co_{0.3}Zn_{0.2}O_4$/CuCr-LDH composite resulted in high photo-Fenton-like oxidation of CAF, it was selected as the photocatalyst for evaluating CAF degradation under different degradation processes (Fig. 5) such as photolysis (just vis-light), HP photoactivation (HP/vis-light), Fenton-like (HP/composite), photocatalysis (vis-light/composite), photo-Fenton-like (HP/composite/vis-light). It is worth noting that CAF removal under dark conditions (adsorption) was lower than 2.7 %, therefore the related results have not been reported in Fig. 5. No direct activation of HP under visible light irradiation was observed as expected, while the photocatalytic and Fenton-like processes raised the degradation rate of CAF to 40.8 and 14.9 %, respectively. The results also confirmed that the presence of visible light resulted in the degradation efficiency of 3 times more than those for the sole Fenton-like process.

The enhanced degradation efficiency in the presence of the visible light source relates to the acceleration of ≡M(III)/≡M(II) and ≡M(II)/≡M(I) cycles by the contribution of photogenerated electrons coming from the excitation of the prepared semiconductor under visible light irradiation (Wu et al., 2020). This enhances the Fenton-like reactions for the production of $^{\bullet}OH$ in the presence of HP. Palanivel et al, (Palanivel et al., 2019) proved that the nanocomposite of $ZnFe_2O_4$ and g-C_3N_4 showed the existence of a synergistic effect for the appropriate degradation of Methylene blue in the presence of HP and under visible light irradiation. According to the authors, the high-performance photo-Fenton-like process had been resulted from the efficient separation of charge carriers and consequently more involvement of electrons in the ≡Fe(III)/≡Fe(II) cycle.

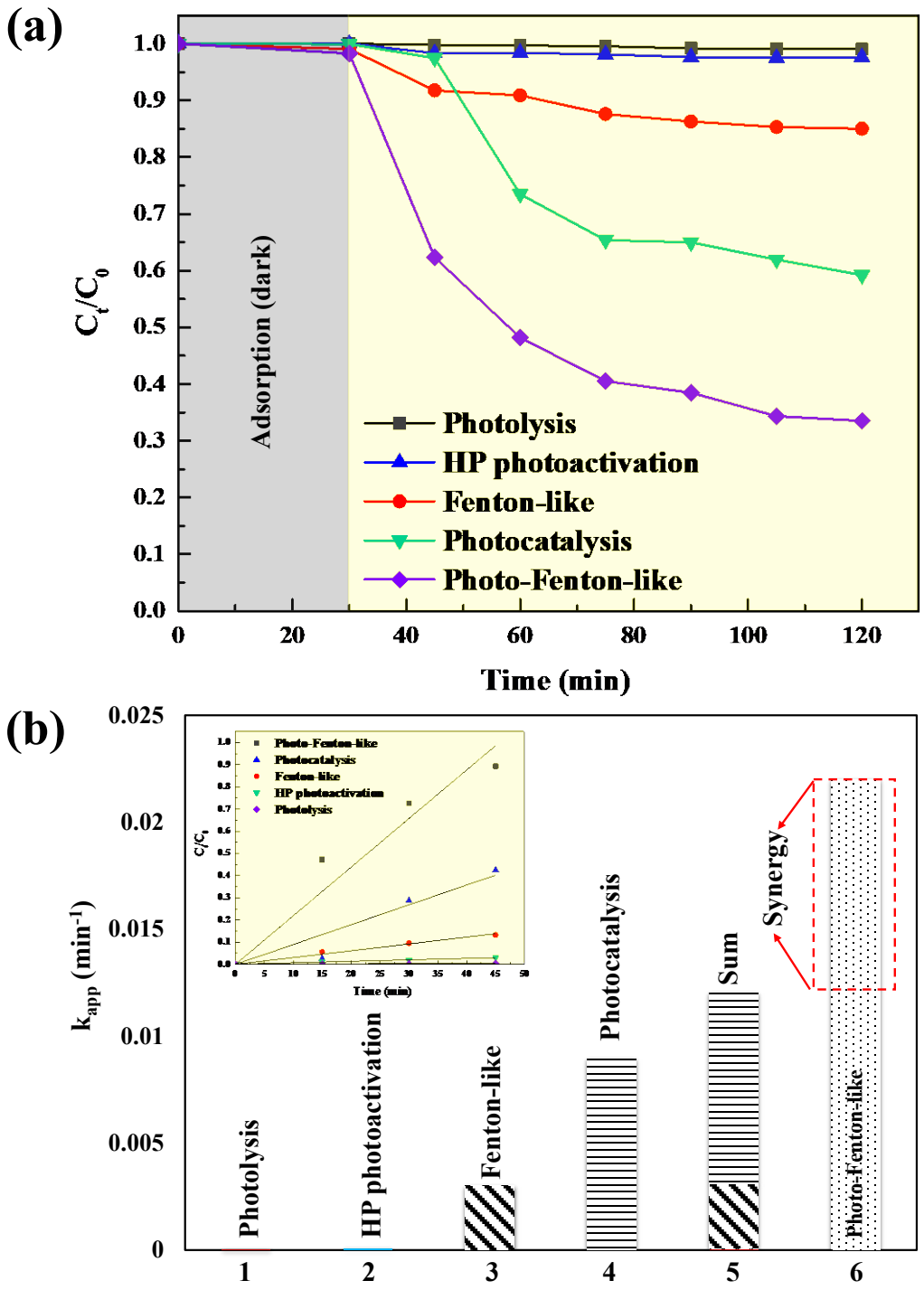

Fig. 5. Degradation of caffeine under different processes (a). Studying the synergestic effect of photo-Fenton-like process using $Fe_{2.5}Co_{0.3}Zn_{0.2}O_4$/CuCr-LDH composite (b). Experimental conditions: composite concentration of 0.5 g L^{-1}, [caffeine] = 50 µM, [H_2O_2 (HP)] = 5 mM and pH = 8.

In the context of water pollutant degradation processes, the existence of a synergy factor is essential (Fazli et al., 2021c). The synergy factor can be defined for those mixed degradation processes which lead to a better degradation efficiency in comparison with the sum of individual processes (Bansal and Verma, 2017). For this purpose, we studied the kinetics of CAF degradation by applying the pseudo-first-order model ($\ln \frac{C_0}{C_t} = k_{app} t$). The obtained correlation coefficient values ($R^2 > 0.9$) for all the processes reveal that the above-mentioned model fits well for the degradation of CAF under the applied photo-Fenton-like process. The rate constants (k_{app}) for different processes have been reported in Table 2.

Table 2. The impact of various processes on the pseudo-first-order rate constants of caffeine degradation.

Processes	**k_{app} (min^{-1})**	**Correlation coefficient (R^2)**
Photolysis	4.1×10^{-5}	0.99
Photoactivation of HP	5.7×10^{-5}	0.99
Fenton-like	0.003	0.99
Photocatalysis	0.008	0.95
Photo-Fenton-like	0.022	0.97

For studying in detail, a synergy factor (equation 1) was defined to determine the extent of the synergy effect of the photo-Fenton-like process compared with the photolysis, photoactivation of HP, Fenton-like, and photocatalytic processes. As a consequence, the calculated synergy factor values for the photo-Fenton-like process were calculated to be 2.2, verifying the enhancing performance in the integrated processes. In our previous work (Fazli et

al., 2021c), we also reported the synergistic effect of persulfate and HP activation using co-doped magnetite.

$$R = \frac{k_{app(photo-Fenton-like)}}{k_{app(photolysis)} + k_{app(HPphotoactivation)} + k_{app(Fenton-like)} + k_{app(photocatalysis)}} \quad (1)$$

3.3. Investigating the influential factors on CAF degradation

Various factors such as the amount of composite, pH, HP concentration, and light source are known to have a significant effect on the Fenton-like and photo-Fenton-like processes (Fazli et al., 2021c). The composite concentration can have a positive or even reverse effect on the performance of different photocatalytic degradation processes (J. E. Yang et al., 2020). Therefore, the relationship between the composite concentration and CAF degradation was evaluated and the results were inserted in Fig. 6 (a). The increased composite concentration from 0.1 g L^{-1} to 0.5 g L^{-1} was accompanied by the enhanced degradation efficiency for CAF. It is assumed that the abundance of the active sites (J. E. Yang et al., 2020), as well as the generation of different reactive free radicals (Fazli et al., 2021a; Rad et al., 2018) in the reaction media, can be the major reason for the degradation of CAF. Nevertheless, beyond the observed increasing trend, the composite concentration of 0.75 g L^{-1} and 1 g L^{-1} displayed an obvious decline for the CAF degradation. In other terms, a higher increase in the amount of composite inhibited the performance of the photo-Fenton-like process. The results obtained by the other researchers are in good agreement with those of ours. Ghasemipour et al. (Ghasemipour et al., 2020) reported that in the case of using 0.7 g L^{-1} of the RGO10%/ZnO20%/MoS_2 composite, the penetration of the utilized light to the surface of the composite decreased which was due to the fact that the reaction media had become opaque.

Since the solution pH is one of the crucial operating parameters affecting the Fenton-like and photo-Fenton-like reactions at the surface of the composite, we evaluated the effect of

different solution pHs on the degradation efficiency of CAF (Fig. 6 (b)). The results revealed that both strong acidic or basic solutions led to lower CAF degradation efficiency. Commonly, the Fenton-like reactions are more likely to occur in the lower pH values (Ye et al., 2021). However, the CAF degradation efficiency was observed to be low in very acidic conditions. Different researchers have also reported a lower performance of the photo-Fenton-like process in strong acidic conditions (Li et al., 2021; Xiaoliang Fan et al., 2021). Moreover, for basic solution, the lower degradation efficiency can be interpreted to I) the formation of less active structures such as $Fe(OH)_n$, and II) the decomposition of HP to O_2 and H_2O (Behrouzeh et al., 2020; Morshed et al., 2020). For basic solutions, This phenomenon restricts the production of different reactive species for the degradation of CAF reduces.

To better interpret the obtained results, the point of zero charges (pH_{pzc}) was measured for the surface of the $Fe_{2.5}Co_{0.3}Zn_{0.2}O_4$/CuCr-LDH composite which is expressed in section (3-6-1) in details (Fig. S8). Based on the obtained results for pH_{pzc} and considering the protonated form of CAF in the lower pHs ($pH < 10.4$) (Li et al., 2005a), the optimum degradation efficiency of CAF occurred at pH 8. Indeed, the repulsion force in $pH < 6$ decreased the occurrence of degradation reactions on the surface of the composite. It is worth noting that in contrast to the homogenous photo-Fenton-like process, our proposed process showed higher performance for the degradation of CAF in the solution pH value of 8; hence, this pH value was selected as the optimum value for the subsequent test.

The impact of different HP concentrations on the degradation efficiency in the photo-Fenton-like process was also studied and the results were presented in Fig. 6 (c). From the results, it can be inferred that when more HP was introduced to the photo-Fenton-like process the degradation of CAF was accelerated. The increased degradation performance of the photo-Fenton-like process can be related to the fact that the composite was able to activate more amount of HP to generate reactive hydroxyl radicals for the degradation of the target pollutants.

However, further increase of HP concentration up to 7.5 and 10 mM didn't show a significant effect to accelerate the degradation efficiency of CAF under the optimal condition. Indeed, when the concentration of HP reaches its critical point, the performance of $^{\bullet}OH$ can be restricted by its reaction with the excessive amount of HP. The results obtained by Yang et al. (Yang et al., 2015) are in accordance with our results illustrated in Fig. 6 (c). They reported that the decomposition of methylene blue was enhanced by increasing the HP concentration from 0.009 M to 0.176 M, whereas, further increasing it to 0.22 M demonstrated an adverse trend for the removal efficiency of methylene blue. To identify that the composite has the major effect on the degradation efficiency of CAF, 5 mM of HP was used for the degradation of CAF in the absence of photocatalyst and presence of the visible light. The results imply that the sole HP is not capable of CAF degradation, while the presence of composite and 5 mM of HP without vis-light brought about 15% of CAF degradation efficiency. Considering the factors mentioned above, we selected the HP concentration of 5 mM as the optimal concentration for the other tests.

Moreover, a set of experiments were fulfilled to assess the effect and contribution of different irradiating lights on the degradation efficiency of CAF during different processes. In this context, a simulated solar light was provided using a Xenon lamp with or without UV-cut-off filter ($\lambda > 400$ nm). As it is clear from Fig. 6 (d), photolysis of CAF has not occurred in the presence of both light sources. Nonetheless, the presence of additional UV light in the simulated solar light enhanced the degradation efficiency of CAF from 2.2, 41.2, and 66.5 % (in the presence of vis-light) to 11.6, 50.1, and 100% for the HP photoactivation, photocatalysis, and photo-Fenton-like degradation processes, respectively. The principal reason for the enhanced degradation efficiency can be ascribed to the presence of UV fraction of the solar light (Li et al., 2018). Taking account of this fact, the so-synthesized photocatalyst can absorb available UV light, which in turn results in the generation of more electron-hole and subsequently more

reactive radical species. Therefore, the more reactive radical species produced in the reaction media, the more CAF degradation achieved. Furthermore, not only can UV light activate HP to produce more amount of $^{\bullet}OH$ (Gabet et al., 2021), it accelerates the reduction of Fe (III) into Fe (II) (iron photolysis) as the essential agent for the Fenton-like reaction (Wu et al., 2020). Wu et al. (Wu et al., 2020) compared the effect of visible and simulated solar light for the Fenton-like degradation of tetracycline hydrochloride. Accordingly, they claimed that the existence of UV light in the simulated solar light boosted the degradation efficiency of the target pollutant from 34.5% to 78.3 %.

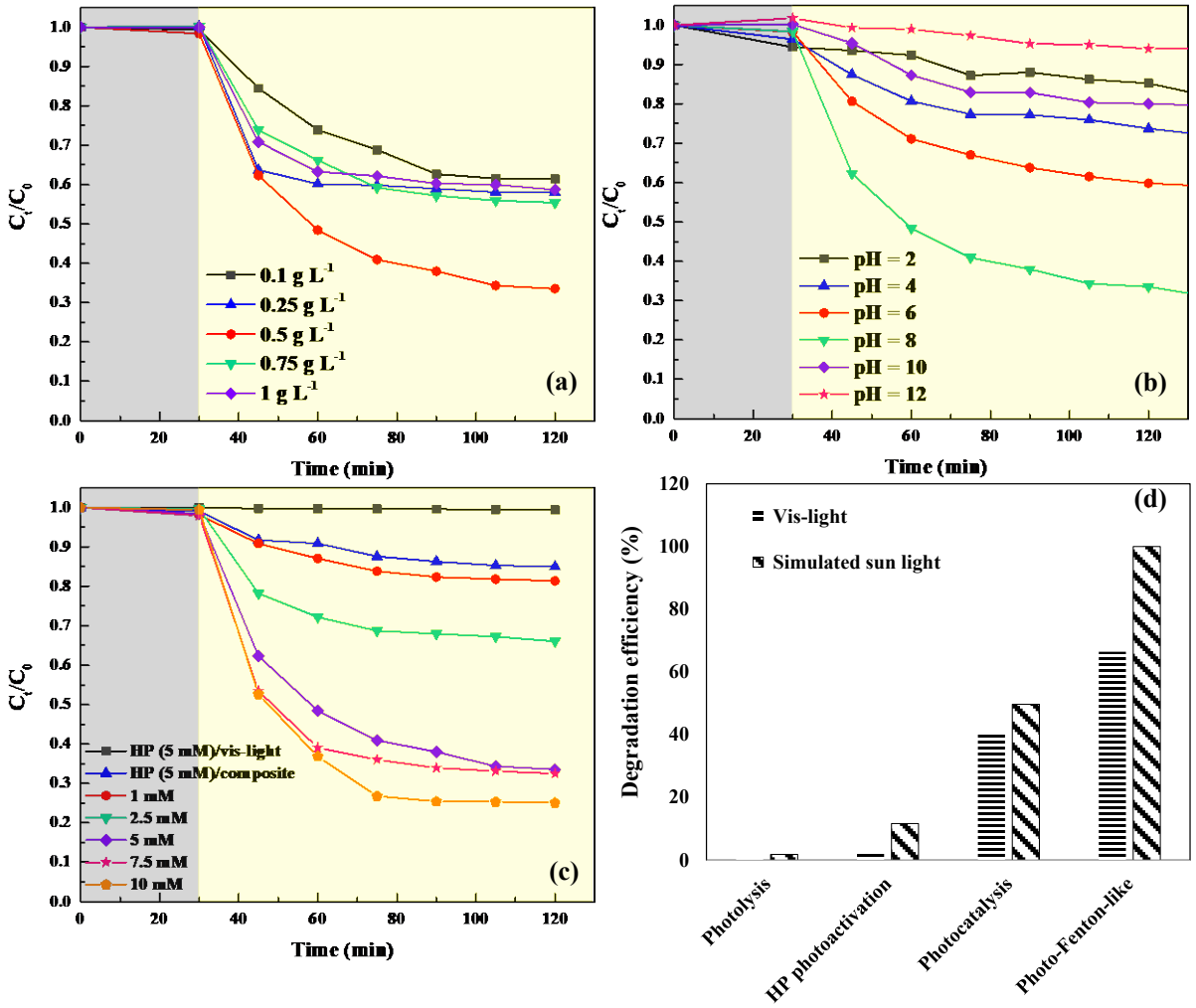

Fig. 6. The effect of (a) composite concentration, (b) initial pH, and (c) H_2O_2 (HP) concentration on the degradation efficiency of caffeine under photo-Fenton-like degradation

process. (d) The effect of different light sources on the performance of various processes. Experimental condition: composite concentration of 0.5 g L^{-1}, [caffeine] = 50 µM, [H_2O_2] = 5 mM and pH = 8.

3.4. The stability and reusability of the photocatalyst

The high photocatalytic activity, as well as a long-term stability of the composite, are the vital factors in the practical applications; hence, the reusability potential of the $Fe_{2.5}Co_{0.3}Zn_{0.2}O_4$/CuCr-LDH composite was tested in 5 cycles of recycling experiments for CAF degradation. According to the results depicted in Fig. S6 (inserted figure), the degradation efficiency of CAF from the first to 5th run decreased from 66.5 to 58.6%. Therefore, comparing with the first cycle, around a 10 % decrease in the CAF degradation efficiency was gained, revealing the persistence of composite stability. Our results in previous work (Fazli et al., 2021c) demonstrated that 5 cycles of the UVA/$Fe_{2.5}Co_{0.3}Zn_{0.2}O_4$/HP process resulted in a 10 % decrease in Sulfalene degradation efficiency. Yang et al. (Yang et al., 2015) reported that 99% of methylene blue was degraded in the cycle of the degradation process; however after six times of using the removal efficiency of the composite reduced to almost 90%.

The stability of the $Fe_{2.5}Co_{0.3}Zn_{0.2}O_4$/CuCr-LDH composite was further proved by comparing the XRD patterns of the freshly provided composite and the composite recycled after 5 times of the degradation process (Fig. S6). The XRD patterns illustrated that the so-synthesized composite did not undergo significant structural variation even after five times of usage. This fact was further verified by ICP analysis, which was applied to determine the concentration of dissolved metal ions from the utilized composite in solution pH of 8. Interestingly, the released concentration of Fe, Co, Zn, Cu, and Cr was attained to be 1.8 µg L^{-1}, 2.1 µg L^{-1}, 1.5 µg L^{-1}, 1.7 µg L^{-1}, and 1.2 µg L^{-1}, respectively. The achieved results were found to be lower than the standard value reported by the World Health Organization (WHO)

(Fazli et al., 2021c, 2021a), indicating the excellent stability of the $Fe_{2.5}Co_{0.3}Zn_{0.2}O_4$/CuCr-LDH composite during the applied degradation process. Therefore, our findings affirmed that the $Fe_{2.5}Co_{0.3}Zn_{0.2}O_4$/CuCr-LDH composite is a stable photocatalyst, which can be used continually in extended environmental applications.

3.5. The effect of inorganic anions and radical scavengers

The existence of different inorganic ions in natural water and wastewater can interfere with the oxidation process of various water contaminants. In this context, different concentrations of chloride and bicarbonate were used to identify their inhibitory impact on the photo-Fenton-like degradation of CAF. As it is clear from Fig. S7 (a), in the case of using 5 and 10 mM of Cl^- a slight decrease (4% and 9%, respectively) in the degradation efficiency of CAF was observed. This effect can be explained considering the complex reaction system starting from the reaction between $^{\bullet}OH$ and Cl^- (reactions 1 to 3). In fact, the formation of less oxidant species such as dichloride radical anion $Cl_2^{\bullet-}$ is only favored under acidic conditions (reaction 2) (Huang et al., 2018a; Khataee et al., 2018).

$$Cl^- + {}^{\bullet}OH \rightleftarrows HOCl^{\bullet-} \quad (1)$$

$$HOCl^{\bullet-} + H^+ \rightleftarrows Cl^{\bullet} + H_2O \quad (2)$$

$$Cl^{\bullet} + Cl^- \rightleftarrows Cl_2^{\bullet-} \quad (3)$$

HCO_3^- is one of the other effective radical scavengers that can convert the highly active hydroxyl radicals to carbonate radicals ($CO_3^{\bullet-}$) (reaction 4).

$$HCO_3^- + {}^{\bullet}OH \rightarrow CO_3^{\bullet-} + H_2O \quad (4)$$

In fact, when we used different concentrations of HCO_3^- ions in the photo-Fenton-like the CAF degradation efficiency was reduced from 66.5% to 58.9% and 52.8% using 5 and 10 mM

of HCO_3^-, respectively. Moreover, our results elucidated that in comparison with chloride the HCO_3^- ions have a slightly stronger inhibiting effect on the degradation of CAF. Liu et al. (Liu et al., 2020) studied the effect of 10 mM of chloride and bicarbonate in the photo-Fenton-like degradation of nitrobenzene in the presence of 8 mM of HP and UV light. They also reported that in comparison with the Cl^- ions, 10 mM of HCO_3^- showed a more inhibiting effect on the degradation of nitrobenzene. Wu et al. (Wu et al., 2017) studied the effect of bicarbonate in the degradation of 4-tert-butylphenol in the course of persulfate activation by Fe (III) species at the solution pH of 8. According to their results, the presence of 2 and 10 mM of bicarbonate resulted in the complete inhibition of 4-tert-butylphenol degradation. Moreover, Tao et al. (Tao et al., 2021) studied the degradation of phenantrene by using UVB activation of hydrogen peroxide. They have also studied the effect of bicarbonate on the phenantrene degradation. According to their results, in the presence of 50 mM of bicarbonate, phenantrene concentration of 10 mg L^{-1}, and at pH of 8, the degradation efficiency of phenantrene was decreased from 33% to almost 16%, indicating a great inhibiting effect of bicarbonate in the presence of homogenous activation of hydrogen peroxide. Heung et al. (Huang et al., 2018b) reported a 50% inhibition of bisphenol A in the presence of 5mM of carbonates and UV-H_2O_2 process. Therefore, it is evident that bicarbonate showed a lower inhibiting effect on CAF during our applied photo-Fenton-like process.

Different scientists such as He et al. reported that $^{\bullet}OH$, superoxide anion radical ($O_2^{\bullet-}$), and photo-generated electron-hole are the primary active species that are responsible for the degradation of organic pollutants through the photo-Fenton-like process. In this regard, isopropanol alcohol (IPA), 4-hydroxy-2,2,6,6-tetramethylpiperidin-1-oxyl (Tempol), chloroform, and KI have been widely used as the appropriate radical scavenger for $^{\bullet}OH$, $O_2^{\bullet-}$, and photogenerated electron and holes, respectively (Fazli et al., 2021c; Jing et al., 2021; Shyamala and Gomathi Devi, 2020). The degradation efficiency of CAF was evaluated in the

absence and presence of the abovementioned radical inhibitors and the results were demonstrated in Fig. S7 (b). Owing to the obtained results, an obvious reduction of CAF degradation efficiency was observed in the presence of IPA, which reveals the participation of reactive $^{\bullet}OH$ in the CAF decomposition. Also, to avoid the probable reaction of $^{\bullet}OH$ with other radical scavengers, IPA with its much higher second-order reaction rate constant ($k_{^{\bullet}OH} = 1.6 \times 10^{9}\ M^{-1}\ s^{-1}$) (Jin et al., 2018) were used in all the following experiments. Therefore, the presence of IPA and tempol brought about an additional 13.5% inhibition in the CAF degradation, which can be effectively ascribed to the contribution of $O_2^{\bullet-}$. On the other hand, chloroform has been reported to react with both $O_2^{\bullet-}$ and photogenerated electrons ($k_{O_2^{\bullet-}} = 2.8 \times 10^{8}\ M^{-1}\ s^{-1}$ and $k_{e^-} = 3 \times 10^{10}\ M^{-1}\ s^{-1}$) (Guo et al., 2021). The holes were capture by the available iodide ion and resulted in decreased degradation extent. However, to remove the possible reaction between chloroform and superoxide or hydroxyl radicals, this experiment has been fulfilled in the presence of tempol and IPA. The reduction was found to be approximately 10.6 %. Chloroform was used to study the participation of photogenerated electrons in the degradation efficiency of CAF. The results showed less contribution of the photogenerated electrons in the decomposition of CAF. Consequently, the active impact of the reactive species can be denoted in the following raising order: $^{\bullet}OH > O_2^{\bullet-} > h^{+} > e^{-}$. The obtained results were similar to the research conducted by Abdelhaleem (Abdelhaleem and Chu, 2020) et al., which used a Fe^{III} impregnated N-TiO_2/HP/visible LED process for the degradation of a pesticide (Carbofuran) from water. They also found out that the photo-Fenton-like degradation process in the presence of Fe (III) impregnated N-TiO_2 resulted in more production and contribution of $^{\bullet}OH$ in the Carbofuran degradation.

3.6. Simultaneous degradation of different water pollutants

554 The effectiveness of the degradation process for the decomposition of different kinds of
555 organic pollutants is of great importance for different scientists (Chavan and Fulekar, 2020;
556 Rimoldi et al., 2017a). Therefore, we studied the photo-Fenton-like degradation of pollutants
557 mixture. With respect to the literature review, BPA and SIM have been classified as water
558 contaminants that are able to create health disorders (Jiang et al., 2020; Sahu et al., 2021).
559 Therefore, besides caffeine as the pharmaceutical water pollution, BPA and SIM were also used
560 as industry and herbicide contaminants. The detailed information of the compounds was given
561 in Table S1.
562
563 **3.6.1. Degradation and mineralization of pollutants mixture**
564 The dark adsorption curves of three target pollutants at the pre-irradiated composite surface
565 illustrated that adsorption/desorption equilibrium was reached less than 5% in 30 min (results
566 were not shown in Fig. 7). Besides, Fig. 7 (a) demonstrates the degradation of pollutants mixture
567 under the photo-Fenton-like degradation process. The results depicted that, the degradation
568 efficiencies of three organic pollutants (SIM, CAF, and BPA) with the total concentration of 25
569 μM were found to be almost 52, 48, and 37 %, respectively. Therefore, the utilized process was
570 found to be more effective for the degradation of SIM and CAF in comparison with BPA. The
571 reason can be ascribed to the reactions which take place on the surface of the composite. With
572 respect to the obtained pH_{pzc} = 5.9 for the composite (Fig. S8), in the case of a greater pH value
573 of the solution ($pH > pH_{pzc}$), the surface would be saturated with the negative charge, while in
574 the acidic solution ($pH < pH_{pzc}$) the surface of the composite would be stuffed with the positive
575 charges (Fazli et al., 2021c). Besides, the dissociation constant (pK_a) of CAF, BPA, and SIM
576 (Lee et al., 2020, p. 4; Li et al., 2005b) have been presented in Fig. S8. Thus, for the solution
577 pH of 8, the surface of the composite is negative which can attract the protonated CAF and the
578 least soluble SIM (6.2 mg L^{-1}) toward the surface of the composite. In the research study
579 belonging to Rimoldi et al. (Rimoldi et al., 2017b), similar results were achieved. They studied

580 the photocatalytic degradation of the mixture containing tetracycline, caffeine, paracetamol,
581 and atenolol in the presence of TiO_2. They reported that among the available pollutants poorly
582 soluble tetracycline showed a higher rate of photocatalytic degradation.

583 The effect of the photo-Fenton-like process on the mineralization of pollutants mixture was
584 investigated with the aim to study the fate of the produced intermediates in the treated water.
585 In this context, an experiment was conducted in the predetermined optimum condition and the
586 TOC removal was reported. The efficiency of the photo-Fenton-like degradation process in
587 terms of the TOC removal for the pollutants mixture was found to be ~ 68% after 4 h of process,
588 respectively. Therefore, the photo-Fenton-like process in the presence of the
589 $Fe_{2.5}Co_{0.3}Zn_{0.2}O_4$/CuCr-LDH composite can be determined as the reliable process for the
590 degradation and long-term mineralization of the pollutants mixture in the solution pH close to
591 the real wastewater. Ghasemipour et al. in their study on the photocatalytic degradation of
592 Aniline reported that at pH solution of 4, and the RGO10%/ZnO20%/MoS_2 concentration of
593 0.7 g L^{-1}, the TOC removal of 40% over the time of 120 min (Ghasemipour et al., 2020). They
594 also reported that more TOC removal of the pollutants mixture was obtained during the longer
595 photocatalytic degradation process.
596

597 ### 3.6.2. Degradation of pollutants mixture in different water bodies

598 In order to study whether the applied photo-Fenton-like process is suitable for practical
599 purposes, the degradation of the pollutant was assessed in different water types. In this regard,
600 we prepared the pollutants mixture solutions in the ultra-pure water, tap water from the
601 University Clermont Auvergne, and real wastewater obtained from the municipal wastewater
602 treatment plant of the Metropole of Clermont-Ferrand, France. The results presented in Fig. 7
603 (b) show that various water matrix resulted in quite different degradation efficiency. A decline
604 in the degradation efficiency of the pollutants in tap water can be related to the inhibition of

produced $^{\bullet}OH$ by HCO_3^- (2.35 mM) that are present in this kind of water. Not only can the hydrogenocarbonate anions occupy the active sites of the photocatalysts to reduce the production of ROS, but also they react with the produced hydroxyl radicals and convert them to the lower oxidative species (reaction 4).

Moreover, Fig. 7 (b) exhibits the accurate comparison for the effect of wastewater matrix on the degradation of three target pollutants. Over 120 min of the process and in the real wastewater, the degradation efficiencies of 34.8%, 36.0%, and 29.2% were respectively found for each of SIM, CAF, and BPA from their mixture solution. The reason for lower efficiency in comparison with those obtained in tap and ultra-pure water mainly depends on the presence of organic matter and inorganic compounds in the real wastewater, which can compete with the available reactive oxygen species such as hydroxyl radical, superoxide radical anion, and photo-generated electron and hole. However, the results undoubtedly show that in the real wastewater, the photo-Fenton-like process in the presence of $Fe_{2.5}Co_{0.3}Zn_{0.2}O_4$/CuCr-LDH composite can degrade more than 30 % of each three water contaminants from their mixture solution, which is good evidence for the efficiency of the proposed performance for the degradation of a wide range of pollutants in the wastewater. Ouyang et al. (Ouyang et al., 2020) declared the same consequence in their research work. They reported that the existence of diverse inorganic and organic substances in the acrylonitrile wastewater reduced the activity of the composite and the generated reactive species during photocatalytic degradation.

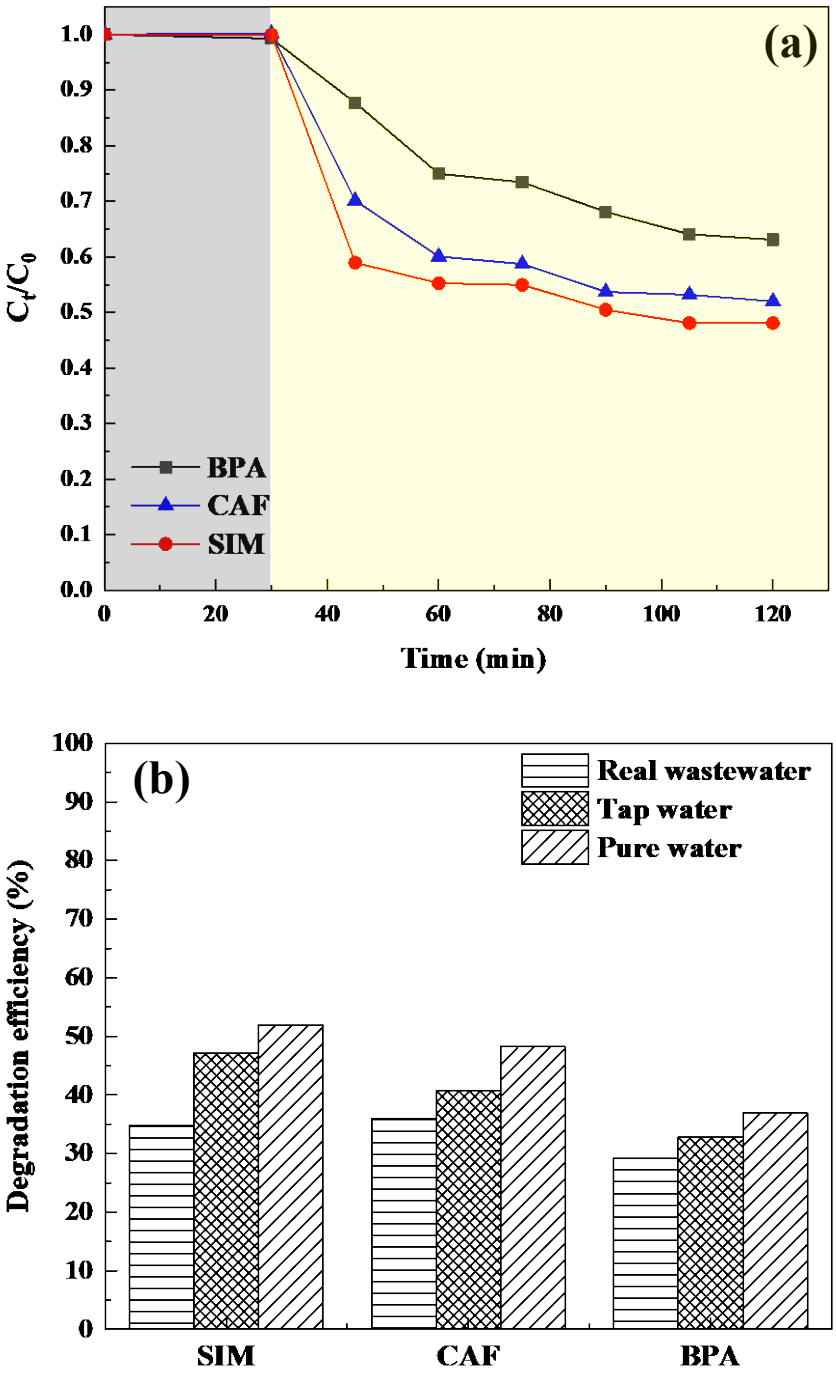

Fig. 7. (a) The adsorption and degradation of simazine (SIM), caffeine (CAF), and bisphenol A (BPA) from their mixture solution in pure water, (b) the effect of different water types on the degradation efficiency of pollutants in their mixture after 120 min of the process. Experimental condition: composite concentration of 0.5 g L^{-1}, total pollutant concentration of 25 µM, $[H_2O_2]$ = 5 mM, and pH = 8.

Conclusion

In this research, a $Fe_{2.5}Co_{0.3}Zn_{0.2}O_4$/CuCr-LDH composite with a well-defined structure was synthesized with a co-precipitation method and its photocatalytic activity was compared with those for Fe_3O_4, CuCr-LDH, $Fe_{2.5}Co_{0.3}Zn_{0.2}O_4$, Fe_3O_4/CuCr-LDH photocatalysts. Thereafter, the synergistic effect of the photo-Fenton-like process for the degradation of an individual pollutant (CAF) was assessed. Furthermore, a set of experiments were fulfilled to study the effect of different composite concentrations, initial pH, HP concentration, and light sources were evaluated. Accordingly, almost 67% of CAF was degraded in the presence of 0.5 g L^{-1} composite concentration, HP (5mM), and at initial solution pH of 8. It was also observed that the used composite preserved its structure and stability even after 5 cycles of successive reactions and it was possible to separate it from the reaction media by applying an external magnetic field. Moreover, in the presence of a simulated solar light without a UV cut-off filter, the degradation efficiency was raised to be 100%. Comparing our results with those published on homogenous photo-Fenton processes, chloride and bicarbonate showed lower inhibiting effects on the degradation of CAF, which is an encouraging result for the future application. Given the results obtained in the presence of different radical scavengers $^{\bullet}OH$ was found to contribute more to the photo-Fenton-like degradation of CAF. In addition, the mixture of CAF, SIM, and BPA was subjected to the photo-Fenton-like degradation process to study their removal efficiency. The TOC removal test depicted the existence of 68% TOC removal of pollutants mixture after 4h of the photo-Fenton-like degradation process. This confirms the complete conversion of the compounds to harmless compounds. Finally, the degradation of a mixture of three contaminates was also investigated in the tap and real wastewater. Although the probable impurities existing in the tap and wastewater reduced the degradation efficiency of the pollutants, more than 30% removal efficiency was achieved for each of the pollutants (> 90 % for total pollutants mixture). In a conclusion, this work shows the feasibility of developing

new visible-light-responsive photocatalysts which reduces the limitation of AOPs such as their pH-dependence, high cost, and generation of secondary pollution with the catalysts.

Acknowledgments

We acknowledge the French Embassy in Iran, the project I-Site CAP 20-25, the program PAUSE of collège de France, and PAI (Pack Ambition Recherche internationale) SOLDE from the Region Auvergne Rhône Alpes for the financial support of Arezou Fazli in this project. Moreover, we would like to thank the Scientific and Technical Research Council of Turkey (TUBITAK, Project Number: 120Y350) for the financial support of the research project. The authors are thankful to Mhammed Banbakkar for conducting the ICP analysis and Dr. Guillaume Monier for accomplishing the XPS analysis.

References

Abdelhaleem, A., Chu, W., 2020. Prediction of carbofuran degradation based on the hydroxyl radical's generation using the FeIII impregnated N doped-TiO_2/H_2O_2/visible LED photo-Fenton-like process. Chem. Eng. J. 382, 122930. https://doi.org/10.1016/j.cej.2019.122930

Aghaziarati, M., Yamini, Y., Shamsayei, M., 2020. An electrodeposited terephthalic acid-layered double hydroxide (Cu-Cr) nanosheet coating for in-tube solid-phase microextraction of phthalate esters. Microchim. Acta 187, 118. https://doi.org/10.1007/s00604-019-4102-5

Alagha, O., Manzar, M.S., Zubair, M., Anil, I., Mu'azu, N.D., Qureshi, A., 2020. Magnetic Mg-Fe/LDH Intercalated Activated Carbon Composites for Nitrate and Phosphate Removal from Wastewater: Insight into Behavior and Mechanisms. Nanomaterials 10, 1361. https://doi.org/10.3390/nano10071361

Bai, J., Liu, Y., Yin, X., Duan, H., Ma, J., 2017. Efficient removal of nitrobenzene by Fenton-like process with Co-Fe layered double hydroxide. Appl. Surf. Sci. 416, 45–50. https://doi.org/10.1016/j.apsusc.2017.04.117

Bansal, P., Verma, A., 2017. Synergistic effect of dual process (photocatalysis and photo-Fenton) for the degradation of Cephalexin using TiO_2 immobilized novel clay beads with waste fly ash/foundry sand. J. Photochem. Photobiol. Chem. 342, 131–142. https://doi.org/10.1016/j.jphotochem.2017.04.010

Behrouzeh, M., Abbasi, M., Osfouri, S., Dianat, M.J., 2020. Treatment of DMSO and DMAC wastewaters of various industries by employing Fenton process: Process performance and kinetics study. J. Environ. Chem. Eng. 8, 103597. https://doi.org/10.1016/j.jece.2019.103597

696 Brillas, E., 2020. A review on the photoelectro-Fenton process as efficient electrochemical
697 advanced oxidation for wastewater remediation. Treatment with UV light, sunlight, and
698 coupling with conventional and other photo-assisted advanced technologies.
699 Chemosphere 250, 126198. https://doi.org/10.1016/j.chemosphere.2020.126198
700 Cao, X.-F., Yue, P., Wei, Q.-R., Dang, Y.-F., Zhang, S.-Q., Wei, Z.-X., Wang, R.-Z., 2021.
701 Synthesis, characterization and catalytic performance of magnetic $La_{0.7}Sr_{0.3}MnO_3$/α-
702 Fe_2O_3 with p–n heterojunction structure. J. Mater. Sci. 56, 7862–7878.
703 https://doi.org/10.1007/s10853-021-05788-3
704 Chavan, A., Fulekar, M.H., 2020. Enhanced degradation efficiency of mixed industrial effluent
705 by modified nanocomposite photocatalyst under UVLED irradiation. Nanotechnol.
706 Environ. Eng. 5, 5. https://doi.org/10.1007/s41204-020-0069-z
707 Chen, F., Huang, G.-X., Yao, F.-B., Yang, Q., Zheng, Y.-M., Zhao, Q.-B., Yu, H.-Q., 2020.
708 Catalytic degradation of ciprofloxacin by a visible-light-assisted peroxymonosulfate
709 activation system: Performance and mechanism. Water Res. 173, 115559.
710 https://doi.org/10.1016/j.watres.2020.115559
711 Chen, H., Hu, L., Chen, M., Yan, Y., Wu, L., 2014. Nickel–Cobalt Layered Double Hydroxide
712 Nanosheets for High-performance Supercapacitor Electrode Materials. Adv. Funct.
713 Mater. 24, 934–942. https://doi.org/10.1002/adfm.201301747
714 Chen, R., Jiang, H., Li, Y.-Y., 2018. Caffeine degradation by methanogenesis: Efficiency in
715 anaerobic membrane bioreactor and analysis of kinetic behavior. Chem. Eng. J. 334,
716 444–452. https://doi.org/10.1016/j.cej.2017.10.052
717 Fazli, A., Brigante, M., Khataee, A., Mailhot, G., 2021a. Synthesis of a magnetically separable
718 LDH-based S-scheme nano-heterojunction for the activation of peroxymonosulfate
719 towards the efficient visible-light photodegradation of diethyl phthalate. Appl. Surf. Sci.
720 149906. https://doi.org/10.1016/j.apsusc.2021.149906

721 Fazli, A., Khataee, A., Brigante, M., Mailhot, G., 2021b. Cubic cobalt and zinc co-doped
722 magnetite nanoparticles for persulfate and hydrogen peroxide activation towards the
723 effective photodegradation of Sulfalene. Chem. Eng. J. 404, 126391.
724 https://doi.org/10.1016/j.cej.2020.126391
725 Gabet, A., Métivier, H., de Brauer, C., Mailhot, G., Brigante, M., 2021. Hydrogen peroxide and
726 persulfate activation using UVA-UVB radiation: Degradation of estrogenic compounds
727 and application in sewage treatment plant waters. J. Hazard. Mater. 405, 124693.
728 https://doi.org/10.1016/j.jhazmat.2020.124693
729 Ghasemipour, P., Fattahi, M., Rasekh, B., Yazdian, F., 2020. Developing the Ternary ZnO
730 Doped MoS_2 Nanostructures Grafted on CNT and Reduced Graphene Oxide (RGO) for
731 Photocatalytic Degradation of Aniline. Sci. Rep. 10, 4414.
732 https://doi.org/10.1038/s41598-020-61367-7
733 Gonçalves, R.G.L., Lopes, P.A., Resende, J.A., Pinto, F.G., Tronto, J., Guerreiro, M.C., de
734 Oliveira, L.C.A., de Castro Nunes, W., Neto, J.L., 2019. Performance of
735 magnetite/layered double hydroxide composite for dye removal via adsorption, Fenton
736 and photo-Fenton processes. Appl. Clay Sci. 179, 105152.
737 https://doi.org/10.1016/j.clay.2019.105152
738 Guo, Y., Zhang, Y., Yu, G., Wang, Y., 2021. Revisiting the role of reactive oxygen species for
739 pollutant abatement during catalytic ozonation: The probe approach versus the
740 scavenger approach. Appl. Catal. B Environ. 280, 119418.
741 https://doi.org/10.1016/j.apcatb.2020.119418
742 Hieu, V.Q., Phung, T.K., Nguyen, T.-Q., Khan, A., Doan, V.D., Tran, V.A., Le, V.T., 2021.
743 Photocatalytic degradation of methyl orange dye by Ti_3C_2–TiO_2 heterojunction under
744 solar light. Chemosphere 276, 130154.
745 https://doi.org/10.1016/j.chemosphere.2021.130154

746 Huang, W., Bianco, A., Brigante, M., Mailhot, G., 2018a. UVA-UVB activation of hydrogen
747 peroxide and persulfate for advanced oxidation processes: Efficiency, mechanism and
748 effect of various water constituents. J. Hazard. Mater. 347, 279–287.
749 https://doi.org/10.1016/j.jhazmat.2018.01.006
750 Jiang, C., Yang, Y., Zhang, L., Lu, D., Lu, L., Yang, X., Cai, T., 2020. Degradation of Atrazine,
751 Simazine and Ametryn in an arable soil using thermal-activated persulfate oxidation
752 process: Optimization, kinetics, and degradation pathway. J. Hazard. Mater. 400,
753 123201. https://doi.org/10.1016/j.jhazmat.2020.123201
754 Jin, Y., Sun, S.-P., Yang, X., Chen, X.D., 2018. Degradation of ibuprofen in water by FeII-
755 NTA complex-activated persulfate with hydroxylamine at neutral pH. Chem. Eng. J.
756 337, 152–160. https://doi.org/10.1016/j.cej.2017.12.094
757 Jing, L., Wang, D., He, M., Xu, Y., Xie, M., Song, Y., Xu, H., Li, H., 2021. An efficient broad
758 spectrum-driven carbon and oxygen co-doped g-C_3N_4 for the photodegradation of
759 endocrine disrupting: Mechanism, degradation pathway, DFT calculation and toluene
760 selective oxidation. J. Hazard. Mater. 401, 123309.
761 https://doi.org/10.1016/j.jhazmat.2020.123309
762 Khataee, A., Fazli, A., Fathinia, M., Vafaei, F., 2018. Removal of diatom Nitzschia sp. cells via
763 ozonation process catalyzed by martite nanoparticles. J. Clean. Prod. 186, 475–489.
764 https://doi.org/10.1016/j.jclepro.2018.03.136
765 Khataee, A., Sadeghi Rad, T., Nikzat, S., Hassani, A., Aslan, M.H., Kobya, M., Demirbaş, E.,
766 2019. Fabrication of NiFe layered double hydroxide/reduced graphene oxide (NiFe-
767 LDH/rGO) nanocomposite with enhanced sonophotocatalytic activity for the
768 degradation of moxifloxacin. Chem. Eng. J. 375, 122102.
769 https://doi.org/10.1016/j.cej.2019.122102

770 Kiziltaş, H., Tekin, T., Tekin, D., 2020. Preparation and characterization of recyclable
771 Fe_3O_4@SiO_2@TiO_2 composite photocatalyst, and investigation of the photocatalytic
772 activity. Chem. Eng. Commun. 0, 1–13.
773 https://doi.org/10.1080/00986445.2020.1743694
774 Lee, G.-J., Lee, X.-Y., Lyu, C., Liu, N., Andandan, S., Wu, J.J., 2020. Sonochemical Synthesis
775 of Copper-doped $BiVO_4$/g-C_3N_4 Nanocomposite Materials for Photocatalytic
776 Degradation of Bisphenol A under Simulated Sunlight Irradiation. Nanomaterials 10,
777 498. https://doi.org/10.3390/nano10030498
778 Li, C., Mei, Y., Qi, G., Xu, W., Zhou, Y., Shen, Y., 2021. Degradation characteristics of four
779 major pollutants in chemical pharmaceutical wastewater by Fenton process. J. Environ.
780 Chem. Eng. 9, 104564. https://doi.org/10.1016/j.jece.2020.104564
781 Li, D., Yu, S.-H., Jiang, H.-L., 2018. From UV to Near-Infrared Light-Responsive Metal–
782 Organic Framework Composites: Plasmon and Upconversion Enhanced Photocatalysis.
783 Adv. Mater. 30, 1707377. https://doi.org/10.1002/adma.201707377
784 Li, Q., Wei, G., Yang, Y., Li, Z., Zhang, L., Shao, L., Lai, S., 2020. Insight into the enhanced
785 catalytic activity of a red mud based Fe_2O_3/Zn–Al layered double hydroxide in the
786 photo-Fenton reaction. Catal. Sci. Technol. 10, 7365–7377.
787 https://doi.org/10.1039/D0CY01539C
788 Li, X.-K., Ji, W.-J., Zhao, J., Wang, S.-J., Au, C.-T., 2005a. Ammonia decomposition over Ru
789 and Ni catalysts supported on fumed SiO_2, MCM-41, and SBA-15. J. Catal. 236, 181–
790 189. https://doi.org/10.1016/j.jcat.2005.09.030
791 Liang, X., Zhong, Y., He, H., Yuan, P., Zhu, J., Zhu, S., Jiang, Z., 2012. The application of
792 chromium substituted magnetite as heterogeneous Fenton catalyst for the degradation
793 of aqueous cationic and anionic dyes. Chem. Eng. J. 191, 177–184.
794 https://doi.org/10.1016/j.cej.2012.03.001

795 Liu, F., Yao, H., Sun, S., Tao, W., Wei, T., Sun, P., 2020. Photo-Fenton activation mechanism
796 and antifouling performance of an FeOCl-coated ceramic membrane. Chem. Eng. J.
797 402, 125477. https://doi.org/10.1016/j.cej.2020.125477
798 Liu, Ying, Liu, Yan, Shi, H., Wang, M., Cheng, S.H.-S., Bian, H., Kamruzzaman, M., Cao, L.,
799 Chung, C.Y., Lu, Z., 2016. Cobalt-copper layered double hydroxide nanosheets as high
800 performance bifunctional catalysts for rechargeable lithium-air batteries. J. Alloys
801 Compd. 688, 380–387. https://doi.org/10.1016/j.jallcom.2016.07.224
802 Morshed, M.N., Pervez, M.N., Behary, N., Bouazizi, N., Guan, J., Nierstrasz, V.A., 2020.
803 Statistical modeling and optimization of heterogeneous Fenton-like removal of organic
804 pollutant using fibrous catalysts: a full factorial design. Sci. Rep. 10, 16133.
805 https://doi.org/10.1038/s41598-020-72401-z
806 Nahim-Granados, S., Rivas-Ibáñez, G., Antonio Sánchez Pérez, J., Oller, I., Malato, S., Polo-
807 López, M.I., 2020. Synthetic fresh-cut wastewater disinfection and decontamination by
808 ozonation at pilot scale. Water Res. 170, 115304.
809 https://doi.org/10.1016/j.watres.2019.115304
810 Nguyen, X.S., Pham, T.D., Vo, H.T., Ngo, K.D., 2021. Photocatalytic degradation of
811 cephalexin by g-C_3N_4/Zn doped Fe_3O_4 under visible light. Environ. Technol. 42, 1292–
812 1301. https://doi.org/10.1080/09593330.2019.1665110
813 Ouyang, F., Li, H., Gong, Z., Pang, D., Qiu, L., Wang, Y., Dai, F., Cao, G., Bharti, B., 2020.
814 Photocatalytic degradation of industrial acrylonitrile wastewater by F–S–Bi–TiO_2
815 catalyst of ultrafine nanoparticles dispersed with SiO_2 under natural sunlight. Sci. Rep.
816 10, 12379. https://doi.org/10.1038/s41598-020-69012-z
817 Palanivel, B., Mudisoodum perumal, S. devi, Maiyalagan, T., Jayarman, V., Ayyappan, C.,
818 Alagiri, M., 2019. Rational design of $ZnFe_2O_4$/g-C_3N_4 nanocomposite for enhanced

photo-Fenton reaction and supercapacitor performance. Appl. Surf. Sci. 498, 143807. https://doi.org/10.1016/j.apsusc.2019.143807

Rad, T.S., Khataee, A., Rahim Pouran, S., 2018. Synergistic enhancement in photocatalytic performance of Ce (IV) and Cr (III) co-substituted magnetite nanoparticles loaded on reduced graphene oxide sheets. J. Colloid Interface Sci. 528, 248–262. https://doi.org/10.1016/j.jcis.2018.05.087

Rimoldi, L., Meroni, D., Falletta, E., Pifferi, V., Falciola, L., Cappelletti, G., Ardizzone, S., 2017a. Emerging pollutant mixture mineralization by TiO_2 photocatalysts. The role of the water medium. Photochem. Photobiol. Sci. 16, 60–66. https://doi.org/10.1039/C6PP00214E

Sahu, R.S., Shih, Y., Chen, W.-L., 2021. New insights of metal free 2D graphitic carbon nitride for photocatalytic degradation of bisphenol A. J. Hazard. Mater. 402, 123509. https://doi.org/10.1016/j.jhazmat.2020.123509

Sharma, K., Raizada, P., Hosseini-Bandegharaei, A., Thakur, P., Kumar, R., Thakur, V.K., Nguyen, V.-H., Pardeep, S., 2020. Fabrication of efficient CuO / graphitic carbon nitride based heterogeneous photo-Fenton like catalyst for degradation of 2, 4 dimethyl phenol. Process Saf. Environ. Prot. 142, 63–75. https://doi.org/10.1016/j.psep.2020.06.003

Shyamala, R., Gomathi Devi, L., 2020. Reduced graphene oxide/SnO_2 nanocomposites for the photocatalytic degradation of rhodamine B: Preparation, characterization, photosensitization, vectorial charge transfer mechanism and identification of reaction intermediates. Chem. Phys. Lett. 748, 137385. https://doi.org/10.1016/j.cplett.2020.137385

Tao, Y., Monfort, O., Brigante, M., Zhang, H., Mailhot, G., 2021. Phenanthrene decomposition in soil washing effluents using UVB activation of hydrogen peroxide and

peroxydisulfate. Chemosphere 263, 127996. https://doi.org/10.1016/j.chemosphere.2020.127996

Wu, C.-K., Yin, M., O'Brien, S., Koberstein, J.T., 2006. Quantitative Analysis of Copper Oxide Nanoparticle Composition and Structure by X-ray Photoelectron Spectroscopy. Chem. Mater. 18, 6054–6058. https://doi.org/10.1021/cm061596d

Wu, Q., Yang, H., Kang, L., Gao, Z., Ren, F., 2020. Fe-based metal-organic frameworks as Fenton-like catalysts for highly efficient degradation of tetracycline hydrochloride over a wide pH range: Acceleration of Fe(II)/ Fe(III) cycle under visible light irradiation. Appl. Catal. B Environ. 263, 118282. https://doi.org/10.1016/j.apcatb.2019.118282

Wu, Y., Li, X., Zhao, H., Yao, F., Cao, J., Chen, Z., Ma, F., Wang, D., Yang, Q., 2022. 2D/2D FeNi-layered double hydroxide/bimetal-MOFs nanosheets for enhanced photo-Fenton degradation of antibiotics: Performance and synergetic degradation mechanism. Chemosphere 287, 132061. https://doi.org/10.1016/j.chemosphere.2021.132061

Wu, Y., Prulho, R., Brigante, M., Dong, W., Hanna, K., Mailhot, G., 2017. Activation of persulfate by Fe(III) species: Implications for 4-tert-butylphenol degradation. J. Hazard. Mater. 322, 380–386. https://doi.org/10.1016/j.jhazmat.2016.10.013

Xiao, J., Lai, J., Li, R., Fang, X., Zhang, D., Tsiakaras, P., Wang, Y., 2020. Enhanced Ultrasonic-Assisted Heterogeneous Fenton Degradation of Organic Pollutants over a New Copper Magnetite (Cu-Fe_3O_4/Cu/C) Nanohybrid Catalyst. Ind. Eng. Chem. Res. 59, 12431–12440. https://doi.org/10.1021/acs.iecr.0c01613

Xiaoliang Fan, Cao, Q., Meng, F., Song, B., Bai, Z., Zhao, Y., Chen, D., Zhou, Y., Song, M., 2021. A Fenton-like system of biochar loading Fe–Al layered double hydroxides (FeAl-LDH@BC)/H_2O_2 for phenol removal. Chemosphere 266, 128992. https://doi.org/10.1016/j.chemosphere.2020.128992

867 Yamashita, T., Hayes, P., 2008. Analysis of XPS spectra of Fe^{2+} and Fe^{3+} ions in oxide
868 materials. Appl. Surf. Sci. 254, 2441–2449.
869 https://doi.org/10.1016/j.apsusc.2007.09.063
870 Yang, J.E., Rossignol, E.D., Chang, D., Zaia, J., Forrester, I., Raja, K., Winbigler, H., Nicastro,
871 D., Jackson, W.T., Bullitt, E., 2020. Complexity and ultrastructure of infectious
872 extracellular vesicles from cells infected by non-enveloped virus. Sci. Rep. 10, 7939.
873 https://doi.org/10.1038/s41598-020-64531-1
874 Yang, X., Chen, W., Huang, J., Zhou, Y., Zhu, Y., Li, C., 2015. Rapid degradation of methylene
875 blue in a novel heterogeneous Fe_3O_4@rGO@TiO_2 -catalyzed photo-Fenton system. Sci.
876 Rep. 5, 10632. https://doi.org/10.1038/srep10632
877 Yang, X., Ding, X., Zhou, L., Fan, H., Wang, X., Ferronato, C., Chovelon, J.-M., Xiu, G., 2020.
878 New insights into clopyralid degradation by sulfate radical: Pyridine ring cleavage
879 pathways. Water Res. 171, 115378. https://doi.org/10.1016/j.watres.2019.115378
880 Ye, Q., Xu, H., Wang, Q., Huo, X., Wang, Y., Huang, X., Zhou, G., Lu, J., Zhang, J., 2021.
881 New insights into the mechanisms of tartaric acid enhancing homogeneous and
882 heterogeneous copper-catalyzed Fenton-like systems. J. Hazard. Mater. 407, 124351.
883 https://doi.org/10.1016/j.jhazmat.2020.124351
884 Zhang, H., Nengzi, L., Wang, Z., Zhang, X., Li, B., Cheng, X., 2020. Construction of
885 Bi_2O_3/CuNiFe LDHs composite and its enhanced photocatalytic degradation of
886 lomefloxacin with persulfate under simulated sunlight. J. Hazard. Mater. 383, 121236.
887 https://doi.org/10.1016/j.jhazmat.2019.121236
888